

A MULTI-WAVELENGTH ANALYSIS OF BINARY-AGN CANDIDATE PSO J334.2028+01.4075

ADI FOORD¹, KAYHAN GÜLTEKIN¹, MARK REYNOLDS¹, MEGAN AYERS^{2,3}, TINGTING LIU⁴, SUVI GEZARI⁴, AND JESSIE RUNNOE¹

¹Department of Astronomy, University of Michigan, 1085 S. Univ., Ann Arbor, MI 48103, USA; foord@umich.edu.

²Department of Physics, Lewis & Clark College, 0615 SW Palatine Hill Rd, Portland, OR 97219, USA

³Maria Mitchell Observatory, 4 Vestal Street, Nantucket, MA 02554, USA and

⁴Department of Astronomy, University of Maryland, College Park, MD 20742, USA

Draft version April 6, 2024

ABSTRACT

We present analysis of the first *Chandra* observation of PSO J334.2028+01.4075 (PSO J334), targeted as a binary-AGN candidate based on periodic variations of the optical flux. With no prior targeted X-ray coverage for PSO J334, our new 40 ksec *Chandra* observation allows for the opportunity to differentiate between a single or binary-AGN system, and if a binary, can characterize the mode of accretion. Simulations show that the two expected accretion disk morphologies for binary-AGN systems are (i) a “cavity,” where the inner region of the accretion disk is mostly empty and emission is truncated blueward of the wavelength associated with the temperature of the innermost ring, or (ii) “minidisks”, where there is substantial accretion from the circum-binary disk onto one or both of the members of the binary, each with their own shock-heated thin-disk accretion system. We find the X-ray emission to be well-fit with an absorbed power-law, incompatible with the simple cavity scenario. Further, we construct an SED of PSO J334 by combining radio through X-ray observations and find that the SED agrees well with that of a normal AGN, most likely incompatible with the minidisk scenario. Other analyses, such as locating the quasar on IR color-color diagrams and analyzing the quasar mass predicted by the fundamental plane of black hole activity, further highlight the similarity of PSO J334 with respect to normal AGN. On the multi-wavelength fronts we investigated, we find no evidence supporting PSO J334 as a binary-AGN system, though our analysis remains insensitive to some binary configurations.

Keywords: galaxies:nuclei — galaxies:active — galaxies:jets — accretion, accretion disk — black hole physics

1. INTRODUCTION

Classical hierarchical galaxy evolution predicts galaxies to merge (e.g., White & Rees 1978), allowing any central supermassive black holes (SMBH) to assemble into binary active galactic nuclei (AGN) systems (Volonteri et al. 2003). The galaxy merger can serve as one possible avenue of growth for the central black holes, and it is expected to end with the coalescence of the two black holes as a result of the emission of gravitational waves (see Begelman et al. 1980). The new SMBH will have a different mass and spin (Rezzolla et al. 2008) and can receive a gravitational recoil large enough to kick it out of the merged host galaxy (e.g., Volonteri et al. 2008; Baker et al. 2008; Merritt et al. 2004; Lousto & Zlochower 2013). As powerful sources of gravitational waves and a likely influence on the BH occupation fraction of galaxies, binary SMBHs are important systems to study.

The process of black hole merging can be broken into distinct phases. Here, we reorganize the original phases presented in Begelman et al. (1980) to emphasize details important to our analysis: (1) the galaxy merger phase, where the two central black holes sink to the center and a bound black hole pair forms with semimajor axis a ; (2) the final parsec phase, where the black hole binary system may or may not stall at a separation of $0.1 \lesssim a \lesssim 1.0$ pc as a result of ejecting all the stars in its loss cone. This phase is referred to as the “final parsec problem” (Milosavljević & Merritt 2003a,b) and many potential solutions have been theorized (e.g., Yu 2002; Escala et al. 2005; Berczik et al. 2006; Mayer et al. 2007; Dotti et al. 2007; Berentzen et al. 2009; Cuadra et al. 2009; Lodato et al. 2009; Khan et al. 2013); (3) the circum-binary accretion phase, where circum-binary accretion is expected as a result of the typical accretion disk size being larger than the

binary separation a (see Milosavljević & Phinney 2005); (4) the gravitational wave phase, where the binary is sufficiently hardened and gravitational waves carry energy from the system until the binary merges (see Peters 1964); and (5) the post-merger phase, where the new black hole has a different mass and spin (Rezzolla et al. 2008), possibly leading to a recoil large enough to displace or eject the black hole from the galaxy center (Volonteri et al. 2008; Baker et al. 2008; Merritt et al. 2004; Lousto & Zlochower 2013).

“Dual-AGN” are usually defined as a pair of AGN with kiloparsec scale separations (i.e., phase 1; see Comerford et al. 2009), while a “binary-AGN” is a pair of BHs that are gravitationally bound with typical separations $a < 100$ pc (i.e., phase 2 & 3; see Bansal et al. 2017 for the first resolved binary-AGN candidate with a separation of ~ 7.3 pc). Such a system becomes impossible to resolve with *Chandra* beyond a distance of ~ 4 Mpc. For example, the closest dual-AGN candidate identified using two resolved point sources with *Chandra* is NGC 3393 (Fabbiano et al. 2011) with a projected separation of ~ 150 pc ($\sim 0''.6$). However, this source has been contested as potentially spurious (e.g., Koss et al. 2015).

Thus many indirect detection techniques have been developed to search for signs of binary-AGN. One such method involves looking for periodic variability in the optical flux via time-domain observations, a possible result of accretion via a circum-binary disk (e.g., D’Orazio et al. 2013; Farris et al. 2015b,a). Perhaps the strongest case of a candidate binary-AGN, OJ 287, was identified by its variable luminosity and has exhibited regular optical outbursts with ~ 12 year period (Lehto & Valtonen 1996). However, OJ 287 is not the typical binary system, as the fluctuations in its lightcurve have been modeled as the secondary SMBH periodically intercepting the primary SMBH’s accretion disk (Valtonen et al. 2008 and ref-

erences therein). Such a model can result from a configuration where there is a considerable misalignment between the orbital plane of the secondary SMBH and the accretion-disk plane of the primary SMBH.

Other quasars have been identified as binary-AGN candidates via time-domain techniques, such as PG 1302–102 (Graham et al. 2015) and PSO J334.2028+01.4075 (hereafter PSO J334; Liu et al. 2015). PG 1302–102 was identified as a binary-AGN based on the periodic variability of the optical flux on an observed timescale of $\sim 1,884$ days, corresponding to a separation of $a \sim 0.01$ pc (Graham et al. 2015). Further, it was argued that the variability of the light curve could be explained by relativistic Doppler boosting from an unequal-mass binary (D’Orazio et al. 2015). Similarly, PSO J334, at a redshift of $z = 2.06$, was identified as a potential binary system based on periodic variation of the optical flux on an observed timescale of ~ 542 days, corresponding to a separation $a \sim 0.006$ pc (Liu et al. 2015). However, recently Vaughan et al. (2016) have shown that the data presented on PG 1302–102 and PSO J334 are not strong enough to support the model of a binary-AGN system. Specifically, they find that sinusoidal variations are difficult to distinguish from a stochastic (“red noise”) process when the number of cycles is ≤ 2 , and that at least ~ 5 cycles are needed to confirm a true periodic trend in lightcurves. In response, Liu et al. (2016) tested the persistence of PSO J334’s periodic lightcurve fluctuations using an extended baseline analysis composed of both archival and new data. This new analysis disfavors a simple sinusoidal model for PSO J334 over a baseline of 5 cycles. Yet, the true nature of PSO J334 remains in question. Recent Karl Jansky Very Large Array (VLA) and Very Long Baseline Array (VLBA) coverage presented in Mooley et al. (2017) further supports that PSO J334 is a binary black hole system, as the quasar was found to be lobe-dominated with a twisted radio structure, a possible result of a precessing jet.

Perhaps the best way to discern between the binary and single-AGN models is to use multi-wavelength observations. With no prior targeted X-ray coverage for PSO J334, our new 40 ksec *Chandra* observation allows for a complete multi-wavelength description of the quasar. Specifically, combining archival data with our new observations may enable us to differentiate between a single or binary-AGN system, and if a binary, can possibly characterize the mode of accretion. If PSO J334 is a binary system with separation $a = 28R_S$ (where $R_S = 2GM/c^2$ is the Schwarzschild radius for a BH with mass M ; Liu et al. 2016) we expect that the binary is well into the gravitational-wave dominated regime, where circum-binary accretion is likely. The mode of circum-binary accretion will depend on the current state of the system. For example, if the specific angular momentum of the streams is small compared to the specific angular momentum at the innermost stable circular orbit (ISCO), the streams will flow directly into the SMBHs (see Gültekin & Miller 2012, Tanaka & Haiman 2013, Tanaka 2013, Gold et al. 2014, Roedig et al. 2014). However, this scenario is expected for SMBHs with very small separations. For all other binary systems, accretion disks form around each SMBH (“minidisks”), extending to a tidal truncation radius that is expected to be less than $\sim a/2$ (Paczynski 1977, also see Roedig et al. 2014 for the dependency of the truncation radius on mass ratio q).

For further-evolved binaries, the timescale to fully accrete the minidisks can be smaller than the gravitational-wave timescale; in this scenario the mini-disks will be drained be-

fore the two SMBHs merge. Here we may expect a cavity between the circum-binary disk and the SMBHs, as the inner regions of the accretion disk are mostly void of gas. The cavity model and the minidisk model are expected to manifest differently in the observational data. For example, one can look at the X-ray spectrum to search for the presence of streams from the circum-binary disk accreting onto the minidisk (e.g., Roedig et al. 2014; Farris et al. 2015b,a). Further, the radio–X-ray AGN spectral energy distribution (SED) can be used to search for abnormalities, such as “notches” in the SED expected from minidisks (however, see Leighly et al. 2016 for a critical perspective on possible “notches” in the SED of Mrk 231), or the presence of a cavity (see Milosavljević & Phinney 2005). Here we present a multi-wavelength analysis of PSO J334, discovered in the FIRST Bright Quasar Survey (Becker et al. 2001), in order to infer its true accretion nature. In the following analysis we assume a standard Λ CDM cosmology of $\Omega_\Lambda = 0.7$, $\Omega_M = 0.3$, and $H_0 = 70 \text{ km s}^{-1}$.

2. X-RAY DATA ANALYSIS

We targeted PSO J334 in Cycle 17 (Proposal ID:17700741, PI: Gültekin). The quasar was placed on the back illuminated S3 chip of the Advanced CCD Imaging Spectrometer (ACIS) detector, with an exposure time of 40 ks. The exposure time was chosen in order to achieve a 3σ point-like source detection, based on an upper-limit calculated from a previous *XMM-Newton* slew survey observation where no emission consistent with the position of PSO J334 was detected, and assuming emission from an active black hole with $L \geq 10^{-3} L_{\text{Edd}}$ with mass $\log(M/M_\odot) = 9.1$ (Liu et al. 2016; Mooley et al. 2017). Our 40 ks exposure is not sensitive to the ~ 542 day optical period found by Liu et al. (2016). Further, our observation is not sensitive to any quasi-periodic signal associated with the decay time from gravitational waves.

We follow a similar data reduction as described in previous X-ray studies analyzing active fractions (Gallo et al. 2008, 2010; Miller et al. 2012b,a, 2015; Plotkin et al. 2014; Foord et al. 2017), using the Chandra Interactive Analysis of Observations (CIAO) v4.8. We first correct for astrometry, cross-matching the *Chandra*-detected point-like sources with the Sloan Digital Sky Survey Data Release 9 (SDSS DR9) catalog. The *Chandra* sources used for cross-matching are detected by running *wavdetect* on the reprocessed level 2 event file. We require each matched pair to be less than $2''$ from one another and have a minimum of 3 matches. Our final astrometrically-corrected image has a shift less than $0''.5$. We then correct for background flaring by removing intervals where the background rate was found to be 3σ above the mean level, resulting in the removal of a 197 second interval. We then rerun *wavdetect* on filtered 0.5 to 7 keV data to generate a list of X-ray point sources. We use wavelets of scales 1, 1.5, and 2.0 pixels using a 1.5 keV exposure map, and set the detection threshold significance to 10^{-6} (corresponding to one false detection over the entire S3 chip). We identify the quasar as an X-ray point source $\sim 0''.4$ from the nominal, SDSS-listed optical center ($2''$ corresponds to 95% of the encircled energy radius at 1.5 keV for ACIS).

All errors evaluated in this paper are done at the 95% confidence level and error bars quoted in the following section are calculated with Monte Carlo Markov Chains via the XSPEC tool chain.

2.1. Spectral Fitting

The quasar’s net count rate and flux value are determined using XSPEC, version 12.9.0 (Arnaud 1996). Counts are extracted from a circular region with radius of $2''$ centered on the X-ray source center, using a source-free annulus with inner radius of $20''$ and outer radius of $30''$ for the background extraction. We fit the spectrum between 0.3 and 7 keV with an absorbed red-shifted power-law (phabs*zphabs*zpow; hereafter Model 1) where we fix the Galactic hydrogen column density (the photoelectric absorption component phabs) to a value¹ of $3.5 \times 10^{20} \text{ cm}^{-2}$. As a result of being in the low-count regime, we implement the Cash statistic (cstat; Cash 1979) and a minimum of 1 count per bin in order to best assess the quality of our model fits. We find the best-fit parameters intrinsic $N_H = 0.91^{+4.84}_{-0.89} \times 10^{22} \text{ cm}^{-2}$ and $\Gamma = 2.02^{+0.83}_{-0.39}$, with an observed 2–10 keV flux of $3.20^{+0.9}_{-1.1} \times 10^{-14} \text{ erg cm}^{-2} \text{ s}^{-1}$, or rest-frame 2–10 keV luminosity of $9.40^{+1.4}_{-1.1} \times 10^{44} \text{ erg s}^{-1}$ at $z = 2.06$ (assuming isotropic emission). K -corrections are not applied to the *Chandra* data, as we directly measure the flux density from the spectrum. In Figure 1, we show the X-ray spectrum of PSO J334 along with the best-fit XSPEC model.

We add a line component to the *Chandra* spectrum (phabs*zphabs*(zpow+zgaus)) to investigate the presence of an Fe K- α line (seen as a slight excess compared to the model at observed-frame 2 keV in Fig. 1). Allowing the line energy to vary, a gaussian component is best-fit at rest-frame $6.2^{+1.2}_{-4.4} \text{ keV}$. We find that the addition of this Fe K- α line is not statistically significant (as is evident from the uncertainties on the line energy) most likely a result of the spectrum only having 196 counts. Further, the placement of the emission line is near a strong drop in effective area of the ACIS-S3 chip, which complicates the study of a potential line. While the Fe K- α line is not statistically significant, we fix the rest-frame energy to 6.4 keV and the width of the line $\sigma = 0 \text{ keV}$, and calculate an equivalent width (EW) of 0.22 keV with a 3σ upper limit of 0.55 keV.

We test for the presence of two accretion disks by fitting a broken power-law to the spectrum (phabs*zphabs*bknpo; Model 2). Such a spectrum may originate from a binary system where both SMBHs are accreting with their own mini-disk. We model the spectrum with a broken power-law in order to avoid the degeneracies that exist in parameter-space for a double power-law model. To properly compare Model 2 to a single disk system, we also fit the spectrum with a broken power-law but tie the two photon index values to one-another (i.e., $\Gamma_1 = \Gamma_2$; Model 3). We note this approach produces best-fit parameters consistent with best-fit parameters of Model 1. We conduct an F-test to investigate the significance of Model 2 with respect to Model 3, and find an f-value of 0.25 (with probability value $p = 0.78$). At a 95% confidence level, we conclude that the spectrum does not need an additional photon index to explain its shape. We note that these results are not necessarily indicative of a single-AGN system, as it is difficult to disentangle two power-laws without predominant spectral features, such as Fe K- α lines at different velocities (a non-negligible scenario, see Eracleous et al. 2012; Popović 2012; Jovanović et al. 2016; Simić & Popović 2016 for more details of emission lines in binary-AGN).

We calculate the X-ray hardness ratio (HR) of PSO J334,

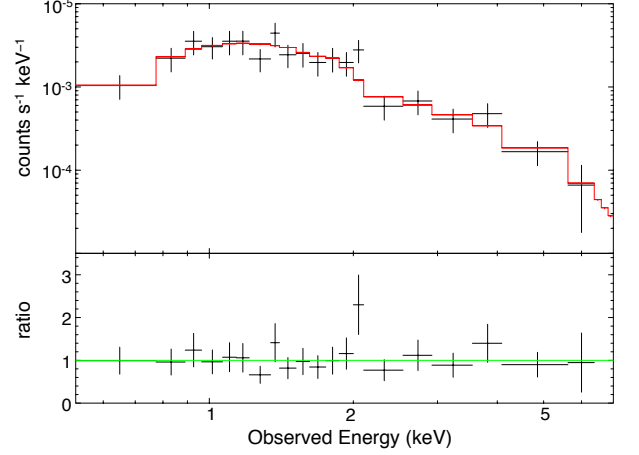


Figure 1. *Top:* The observed 0.3 – 7.0 keV *Chandra* spectrum of PSO J334 is shown in black, where the data have been folded through the instrument response. We fit the spectrum with the model phabs*zphabs*zpow, fixing the Galactic absorption and redshift parameters at $N_H = 3.5 \times 10^{20} \text{ cm}^{-2}$ and $z = 2.06$. The best-fit model is shown in red, where intrinsic $N_H = 0.91^{+4.84}_{-0.89} \times 10^{22} \text{ cm}^{-2}$ and $\Gamma = 2.02^{+0.83}_{-0.39}$. We calculate an observed 2–10 keV flux of $3.20^{+0.9}_{-1.1} \times 10^{-14} \text{ erg cm}^{-2} \text{ s}^{-1}$, or rest-frame 2–10 keV luminosity of $9.40^{+1.4}_{-1.1} \times 10^{44} \text{ erg s}^{-1}$ at $z = 2.06$ (assuming isotropic emission). All errors are evaluated at the 95% confidence level. *Bottom:* Ratio of the data to the continuum model for PSO J334. We find that at a 95% confidence level, the spectrum does not need an additional power-law to explain the data. The spectrum has been rebinned for plotting purposes.

defined as $(H-S)/(H+S)$ where S and H are the soft (0.5–2.0 keV) and hard (2.0–8.0 keV) X-ray band net counts detected by *Chandra*. The HR is found to be ~ 0.40 , consistent with the expected value for an AGN with $N_H \simeq 10^{22} \text{ cm}^{-2}$ and $z \simeq 2.06$ (e.g. Wang et al. 2004).

3. THE SPECTRAL ENERGY DISTRIBUTION

In the following section we construct a spectral energy distribution of PSO J334, by combining radio to X-ray observations, and compare it to standard non-blazar AGN SEDs presented in Shang et al. (2011). For all K -corrections, we adopt the $K(z)$ relation as presented in Richards et al. (2006).

3.1. Radio

PSO J334 has archival spectroscopy from the FIRST Bright Quasar Survey (FBQS), and has recently been re-observed by the VLA as part of the Caltech-NRAO Stripe 82 Survey (Mooley et al. 2016). Further, Mooley et al. (2017) present VLBA observations of PSO J334 at 7.40, 8.67, and 15.37 GHz, respectively. Two VLBA components are resolved—a South East and a North West component. Both the compactness and the inverted radio spectrum of the South East component (possibly due to synchrotron self-absorption) suggest that it is the “core” from which the North West component has been ejected. For the purposes of constructing the SED, we use the VLBA integrated flux density values for the South East component (see table 3 in Mooley et al. 2017). K -corrections for the radio data points are implemented assuming a spectral index $\alpha = -0.3$ with a dispersion 0.2 (where $F_\nu \propto \nu^{-\alpha}$). The value for α is taken from Stocke et al. (1992), and represents the radio slope of the average quasi-stellar object (QSO) SED, which includes contributions from both the core and lobes.

3.2. Infrared

¹ We evaluate the neutral hydrogen column density using values from the Leiden/Argentine/Bonn (LAB) Survey of Galactic HI (Kalberla et al. 2005) via WebPIMMS.

For the infrared regime we use archival *Wide-field Infrared Survey Explorer* (WISE) from the AllWISE Source Catalog (Cutri et al. 2013), as well as stacked archival *J*- and *K*-band data from the UKIRT InfraRed Deep Sky Survey (UKIDSS; Lawrence et al. 2007). For the WISE data we use observations taken in the W1, W2, and W3 bands, where the quasar was detected with a SNR > 3.0. We correct for Galactic extinction using the dust map from Schlafly & Finkbeiner (2011), where $E(B - V) = 0.0401$. *K*-corrections are applied assuming a spectral index $\alpha = -1.0$ with a dispersion of 0.2, calculated from the average 1–10 μm spectral index for the AGN sample presented in Shang et al. (2011).

3.3. Optical

PSO J334 has archival *g*-, *r*-, *i*-, and *z*-band data from the Pan-STARRS1 Medium Deep Survey (PS1 MDS; Kaiser et al. 2010), *V*-band data from the Catalina Real-time Transient Survey (CRTS; Drake et al. 2009), and archival *u*-, *g*-, *r*-, *i*-, and *z*-band data from the Sloan Digital Sky Survey (SDSS). For the purposes of constructing our SED, we use magnitudes extracted from deep stacked images in the *g*-, *r*-, *i*-, and *z*-bands from PS1 MDS (Liu et al. 2015, 2016). Similar to the IR regime, we correct for Galactic extinction using the dust map from Schlafly & Finkbeiner (2011). For the PS1 MDS *K*-corrections, we follow Liu et al. (2015) and assume a spectral index $\alpha = -0.5$ with a dispersion of 0.3 (also see Elvis et al. 1994; Vanden Berk et al. 2001; Ivezić et al. 2002).

3.4. Ultraviolet

PSO J334 has *u*-band data from the Canada-France-Hawaii Telescope (CFHT; Heinis et al. 2016a,b; Liu et al. 2016) and archival *Galaxy Evolution Explorer* (GALEX) data in both the FUV and NUV bands. Further, the quasar has GALEX Time Domain Survey data in the NUV, taken to analyze possible periodic variations in the UV lightcurve (Gezari et al. 2013; Liu et al. 2015, 2016). For our SED we use magnitudes derived from deep stacked *u*-band CFHT data and the archival FUV and NUV GALEX data. To account for Galactic absorption in the CFHT data we use the dust map from Schlafly & Finkbeiner (2011), while for the GALEX observations we use FUV and NUV extinction values listed in Yuan et al. (2013). As all data points are shortward of the Ly α emission line, we apply *K*-corrections using the spectral index $\alpha = -1.57$ and a dispersion of 0.17 (Telfer et al. 2002; Richards et al. 2006).

3.5. The Multi-wavelength SED

In Fig. 2 we present the rest-frame multi-wavelength SED of PSO J334 in νL_ν (erg s $^{-1}$) versus frequency (Hertz), assuming a luminosity distance $d_L = 16.1$ Gpc at $z = 2.06$. We search for any abnormalities in the SED by comparing our data to the composite non-blazar AGN SEDs presented in Shang et al. (2011). The composite SEDs are based on a sample of 85 optically bright non-blazar quasars, composed of 27 radio-quiet and 58 radio-loud quasars. Most objects in the sample have quasi-simultaneous UV/optical data, while radio, IR, and X-ray data are obtained from either the literature or new observations. Both the radio-quiet and radio-loud composite SEDs are overplotted with PSO J334's data in Fig. 2. We normalize the flux density of our data to rest-frame $\lambda = 2000$ Å for comparison to the standard AGN SEDs. The luminosities for each rest-frame frequency are listed in Table 1.

Table 1
Spectral Energy Density Values

Filter or Detector (1)	Telescope or Survey (2)	log ν (log(Hz)) (3)	log νL_ν (log(erg s $^{-1}$)) (4)
...	VLBA	10.35	-3.12 ± 0.11
...	VLBA	10.42	-2.80 ± 0.11
...	VLBA	10.67	-2.96 ± 0.13
W3	WISE	13.88	-0.02 ± 0.13
W2	WISE	14.30	-0.14 ± 0.05
W1	WISE	14.44	-0.20 ± 0.05
<i>J</i>	UKIDSS	14.62	-0.03 ± 0.13
<i>K</i>	UKIDSS	14.87	0.18 ± 0.13
<i>z</i>	PS1 MDS	15.03	0.15 ± 0.29
<i>i</i>	PS1 MDS	15.18	0.14 ± 0.29
<i>r</i>	PS1 MDS	15.09	0.16 ± 0.29
<i>g</i>	PS1 MDS	15.28	0.28 ± 0.29
<i>u</i>	CFHT	15.40	0.56 ± 0.23
NUV	GALEX	15.61	0.21 ± 0.22
FUV	GALEX	15.78	0.41 ± 0.19
ACIS-S3	Chandra	17.68–18.38	$-0.87^{+0.06}_{-0.05}$

Note. – Columns: (1) filter or detector; (2) telescope, denoted as the Very Large Baseline Array (VLBA); the *Wide-field Infrared Survey Explorer* (WISE); the UKIRT InfraRed Deep Sky Survey (UKIDSS); the Pan-STARRS1 Medium Deep Survey (PS1 MDS); the Canada-France-Hawaii Telescope (CFHT); the *Galaxy Evolution Explorer* (GALEX); and the *Chandra X-ray Observatory* (3) rest-frame frequency assuming a redshift of $z = 2.06$, in units of Hz. The *Chandra* frequency range corresponds to the rest-frame energy range of 2–10 keV; (4) extinction- and *K*-corrected luminosity assuming a luminosity distance $d_L = 16.1$ Gpc, in units of erg s $^{-1}$. Values have been normalized to the luminosity at rest-frame $\lambda = 2000$ Å. Error bars are evaluated at the 95% confidence level. Please see Section 3 for details on extinction values and *K*-corrections applied.

A simple comparison between the data and the Shang et al. (2011) SEDs shows a good agreement between PSO J334's emission and that of a radio-quiet AGN. The classical definition of radio-quiet quasars are AGN that have $R = f(5 \text{ GHz})/f(4400 \text{ Å}) < 10$, where $f(5 \text{ GHz})$ is the rest-frame flux density at 5 GHz and $f(4400 \text{ Å})$ is the rest-frame flux density at 4400 Å (Kellermann et al. 1989). Above $R = 10$, AGN are usually classified as radio-loud. Results from Becker et al. (2001) identify PSO J334 as a radio-loud quasar, with $R \sim 200$. We use the new 7.40 GHz observations of the South East component of PSO J334 from Mooley et al. (2017), where the resolution has increased from the previous FBQS observations, and derive an R value of ~ 17 (similar to Becker et al. 2001, we assume the radio spectrum follows $f \propto \nu^{-0.5}$ to extrapolate the rest-frame 5 GHz flux density). Although PSO J334 is technically defined as a radio-loud AGN, $R \sim 17$ is decidedly between the radio-loud sample SED from Shang et al. (2011) (where the median $R \sim 1600$) and the radio-quiet sample SED (where the median $R \sim 0.3$). Besides the radio regime, there is substantial overlap between PSO J334's SED and the Shang et al. (2011) data at all other wavelengths.

4. RESULTS AND DISCUSSION

Past studies of PSO J334 have revealed various results regarding the accretion mode of the quasar, as analyses in different wavelength regimes have suggested both single- and binary-AGN systems. PSO J334 was first targeted as a binary-

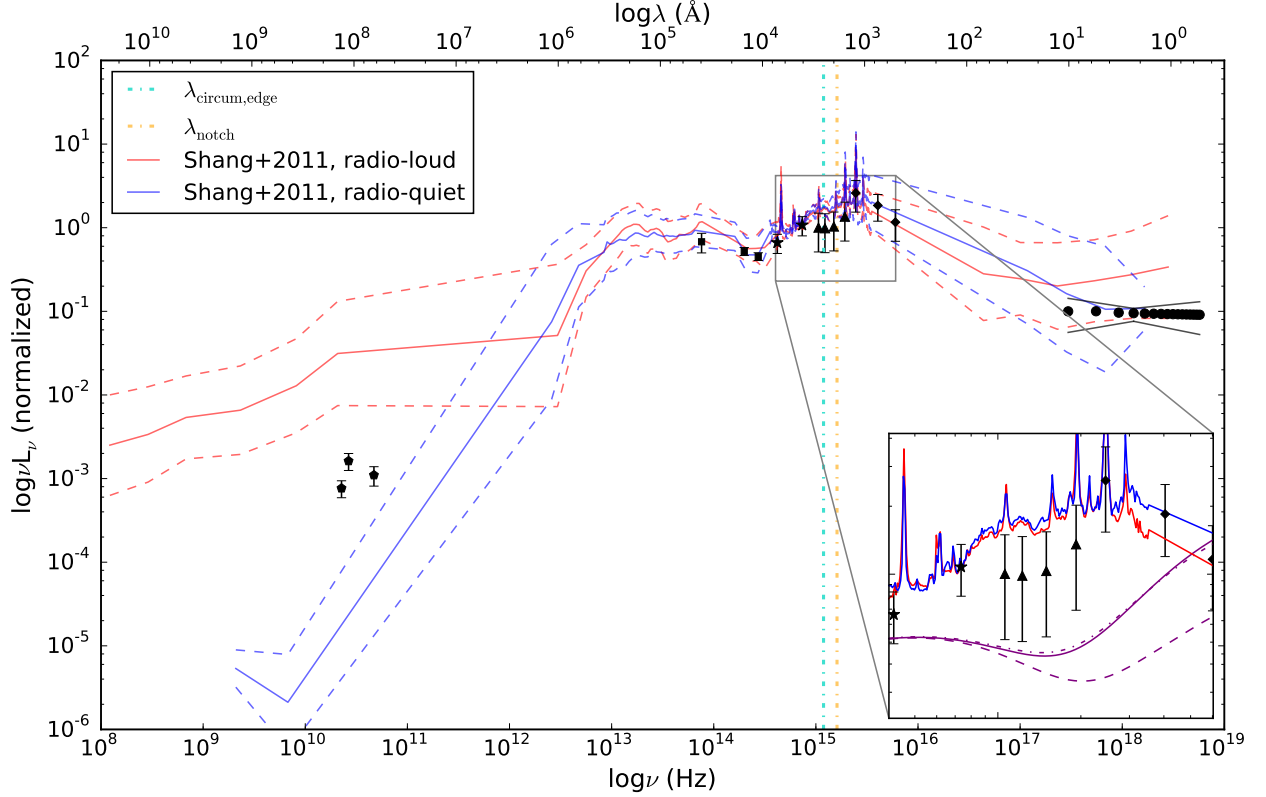


Figure 2. Rest-frame SED of PSO J334. Radio data are from the VLA (black hexagons), IR data are from *WISE* (black-filled squares) and UKIDSS (black-filled stars), optical data are from Pan-STARRS1 (black-filled triangles), UV data are from CFHT and *GALEX* (black-filled diamonds), and X-ray data are from *Chandra* (black-filled stars). Errors on data points are evaluated at the 95% confidence level. We overplot the composite non-blazar AGN SEDs presented in Shang et al. (2011), for both radio-loud (red line) and radio-quiet (blue line) AGN (1σ error bars are denoted by dashed lines). We normalize the flux density of our data to rest-frame $\lambda = 2000$ Å. We indicate $\lambda_{\text{circum,edge}} = 2500$ Å, the wavelength that corresponds to the emission emitted at the inner-edge of a possible circum-binary accretion disk at $R_{\text{circum,edge}} = 2a$ (assuming blackbody radiation), with a cyan dot-dashed line. If PSO J334 were consistent with the cavity model, we do not expect much emission at wavelengths with energies higher than $\lambda_{\text{circum,edge}}$. We also indicate the predicted center wavelength for a notch at $\lambda_{\text{notch}} = 1900$ Å, predicted to range between 500 Å and 7000 Å for a mass ratio $0.3 < q < 1.0$. If PSO J334 were consistent with the minidisk model, we expect a dip in the thermal continuum in this region. The inset shows how the SED is expected to change with the addition of a notch, where we use the analytical calculations derived in Roedig et al. (2014) to illustrate a notched SED with i) $q = 1.0$, $f_1 = f_2 = 0.5$ (purple solid curve), ii) $q = 0.3$, $f_1 = 0.45$, $f_2 = 0.55$ (purple dash-dot curve, and iii) $q = 0.1$, $f_1 = 0.92$, $f_2 = 0.08$ (purple dashed curve). The continuum for the notch is estimated by approximating the Shang et al. (2011) SED between 500 Å and 7000 Å in log space with a straight line. We note that although PSO J334 appears to be better aligned with the radio-quiet sample, the quasar is technically considered to be radio-loud with $R \sim 17$.

AGN candidate based on periodic variation of the optical flux (Liu et al. 2015). Assuming that the rest-frame period of the quasar variability traced the orbital period of the binary, a binary separation of ~ 0.006 pc was estimated. However, recently Vaughan et al. (2016) have shown that sinusoidal variations are difficult to distinguish from a stochastic process when the number of cycles is ≤ 2 ; they conclude that at least ~ 5 cycles are needed to confirm a true periodic trend in lightcurves. Searching for sinusoidal variations in candidate binary-AGN lightcurves is complicated by the fact that binary-AGN are likely to show both periodic and stochastic variations. This is a result of regular quasar variability overlapping with any modulation resulting from being in a binary system. More complex analyses will be necessary for future studies of candidate binary-AGN lightcurves, as it is still relatively uncertain how to best model quasar noise power spectra.

Liu et al. (2016) confirmed that the data disfavored a simple sinusoidal model using an extended baseline analyses composed of both new and archival data in optical and UV. However, most recently Mooley et al. (2017) have re-established the idea of PSO J334 being a binary-AGN system via new

VLA and VLBA observations. The central radio “core” of the quasar was found to have an elongation position angle (PA) twisted by $\sim 39^\circ$ with respect to the elongation PA measured by the VLA on kiloparsec scales. Such twists have been modeled in 3C 207 as a result of a precessing jet, possibly due to the orbital motion associated with binary-AGN (see Hough 2013). However, if the jet axis is close to our line of sight, the PAs may appear amplified as projected onto the plane of the sky. Such a scenario may be relevant to PSO J334, which has been identified as a Type I quasar via broadened CIV (1549 Å) and Mg II (2798 Å) lines (Liu et al. 2015, 2016; Mooley et al. 2017).

With no prior targeted X-ray coverage for PSO J334, our new 40 ksec *Chandra* observation allows for a complete multi-wavelength description of the quasar. Specifically, combining radio–X-ray observations enables us to differentiate between a single or binary-AGN system, and if a binary, can possibly characterize the mode of accretion. Simulations show that the two most basic types of accretion disk morphologies for binary-AGN systems are a cavity, where the inner region of the accretion disk is mostly empty and emission is truncated blueward of the wavelength associated with the temperature

of the innermost ring, or minidisks, where there is substantial accretion onto one or both of the members of the binary, each with their own shock-heated thin-disk accretion system. In the following section we will discuss the implications of our *Chandra* observation and investigate the possibility of PSO J334 being a binary-AGN in terms of the cavity and mini-disk models.

4.1. The Null Hypothesis: PSO J334 is a single-AGN

We first consider analyses which are used to identify normal AGN. Due to the high redshift of PSO J334 standard emission line diagnostics, including narrow emission line ratios (e.g., Kewley et al. 2006) or broad H α emission (e.g., Greene & Ho 2005), are redshifted into the near-infrared where archival spectroscopic data are not available. However, the good agreement between PSO J334’s SED and the non-blazar AGN SEDs presented in Shang et al. (2011) strongly suggests a single-AGN system.

We compute the IR colors of PSO J334, as IR colors are often used as a tool to identify AGN (Jarrett et al. 2011; Stern et al. 2012), although red IR colors can also be produced when dust is heated by recent star formation. Specifically, we determine the position of PSO J334 on a *WISE* color–color plot to (i) determine whether it meets the AGN IR criteria, and (ii) determine if there are any abnormalities in its placement with respect to a normal AGN. We compare PSO J334’s *WISE* colors to the “AGN box” empirically defined by Jarrett et al. (2011), which is based on the colors of quasi stellar objects (QSOs) and Seyfert galaxies with redshift out to $z \sim 2$. With $W1 - W2 = 1.13 \pm 0.11$ and $W2 - W3 = 3.26 \pm 0.27$, PSO J334 has IR colors located within the AGN box of Jarrett et al. (2011) and does not seem to have any IR color abnormalities compared to other QSOs at similar redshifts. However, it is not clear if binary-AGN would differ from a standard AGN in IR color-color diagrams (see Ellison et al. 2017 for an example where a candidate dual-AGN has *WISE* colors consistent with a standard AGN).

Secondly, our *Chandra* observations allows us to look at the location of PSO J334 on the Fundamental Plane of Black Hole Activity (FP)—an empirical relationship between the black hole mass, 5 GHz luminosity $L_{5\text{GHz}}$, and 2–10 keV luminosity L_X . Gültekin et al. (2009) fit a relation to be used as an estimation for black hole mass based on observations of L_X and $L_{5\text{GHz}}$ of the form:

$$\log\left(\frac{M}{10^8 M_\odot}\right) = 0.19 + 0.48 \log\left(\frac{L_{5\text{GHz}}}{10^{38} \text{ erg s}^{-1}}\right) - 0.24 \log\left(\frac{L_X}{10^{40} \text{ erg s}^{-1}}\right). \quad (1)$$

Whether or not the local FP relation is appropriate for high accretion rate AGNs remains a topic of debate. For example, Gültekin et al. (2009) studied a sample of AGN with dynamical black hole mass estimates and uniform analysis of archival *Chandra* data, and confirmed that the inclusion of high-accretion rates sources, such as Seyfert galaxies, increased the intrinsic scatter about the FP. However, other analyses reflect that the FP may be applicable for high accretion-rate sources (e.g., Panessa et al. 2007; Gültekin et al. 2014). Recognizing the caveats of such an analysis, we use the results of Gültekin et al. (2009) to calculate the projected mass of the system and compare it to the measured total mass of the system, which we take to be $\log(M/M_\odot) = 9.1$ (Liu et al. 2016; Mooley et al. 2017). Binary-AGN with small mass ratios may result in offsets from the FP if the secondary is the main accretor—the mass calculated via the FP relation may

be smaller compared to mass of the entire system, reflecting that the coupled X-ray/Radio emission stems from the less massive secondary. However, because of the large scatter on the calculated mass via the FP relation of ~ 1 dex, this approach is only sensitive to the more extreme mass ratio values, e.g. $q \lesssim 0.01$. We find that the mass projected from the FP relation of Gültekin et al. (2009) is consistent, within the error bars, with the entire mass of the system.

4.2. Binary-AGN models

4.2.1. A Cavity in the Circum-binary Disk

If PSO J334 were consistent with the cavity model, the radiation that a normal disk would radiate within the inner edge of the circum-binary disk, $R_{\text{circum,edge}}$, will be missing. The exact values of the temperatures we deduce below depend on details regarding the micro-physics of the system; here we make rough estimates using a standard accretion disk model. Assuming a thin-disk model, a mass ratio not much less than unity (e.g., $q > 0.01$), and an inner edge located at $R_{\text{circum,edge}} \simeq 2a$ (Milosavljević & Phinney 2005), the temperature at the inner edge of the circum-binary disk is given by: $T_{\text{circum,edge}} \simeq 1.96 \times 10^4 [\dot{m}(\eta/0.1)^{-1} M_8^{-1} (a/100 R_G)^{-3}]^{1/4}$ K (Roedig et al. 2014). Here, \dot{m} is the accretion rate in Eddington units, η is the accretion efficiency, M_8 is the total mass of the binary in units of $10^8 M_\odot$, and a is the separation between the two BHs in units of gravitational radius R_G ($R_G = GM/c^2$). In the case of a cavity, we do not expect much emission at temperatures above $T_{\text{circum,edge}}$. We note that this temperature is not predicted to change late into the evolution of the binary where the orbital time becomes smaller than the inflow time of the circum-binary disk, a scenario that may be very relevant to PSO J334 given the calculated separation between the SMBHs listed in Liu et al. (2016).

To calculate $T_{\text{circum,edge}}$ we consider the parameters $\eta = 0.1$, $\log(M/M_\odot) = 9.1 \pm 0.3$ (Mooley et al. 2017), and $a = 28 \pm 14 R_S = 56 \pm 28 R_G$ (Liu et al. 2016). We calculate the accretion rate in Eddington units as $\dot{m} = \dot{M}/\dot{M}_{\text{Edd}} \approx \dot{M}[3 \times 10^{-8} (M/M_\odot) M_\odot \text{ yr}^{-1}]^{-1} \approx 0.26 \pm 0.1$. Here $\dot{M} = L_{\text{bol}}/(\eta c^2)$, where L_{bol} is the bolometric luminosity of the circum-binary accretion disk and is determined from the quasar bolometric luminosity corrections presented in Runnoe et al. (2012), using the quasar’s continuum flux density at $\lambda = 3000 \text{ \AA}$ presented in Liu et al. (2016).

$T_{\text{circum,edge}}$ is found to be $\simeq 11000 \pm 4000 \text{ K}$, or a cut-off wavelength $\lambda_{\text{circum,edge}} \simeq 2500_{-700}^{+1600} \text{ \AA}$ assuming blackbody radiation from the circum-binary accretion disk. We indicate the position of $\lambda_{\text{circum,edge}}$ on PSO J334’s SED in Fig 2. If PSO J334 were consistent with the cavity accretion model, we would expect emission with energies higher than $\sim \text{NUV}$ to be either (i) significantly lower than expected from a normal AGN disk or (ii) disappear entirely. However, if PSO J334 were consistent with a single-AGN system, we would expect UV emission from the inner-most part of the accretion disk that upscatters to X-rays via inverse-Compton interactions with the corona. Combining our 2–10 keV detection and the *GALEX* archival data, we can verify that the X-ray intensity is consistent with the expected upscattered UV emission from a normal AGN disk, reflected by the considerable overlap between PSO J334’s SED and the Shang et al. (2011) data in Fig. 2. We conclude that PSO J334 is incompatible with the cavity scenario.

4.2.2. “Notches” from a Minidisk

Regarding the minidisk model, the radiation that an ordinary disk would radiate between the inner edge of the circum-binary disk and the tidal truncation radii of the minidisks, R_{tidal} , will be missing. In such a scenario, it is expected that the missing emission will produce a dip, or a “notch”, in the thermal continuum spectrum, reflecting the missing emission between $R_{\text{circum,edge}}$ and R_{tidal} (e.g. Roedig et al. 2012; Tanaka et al. 2012; Gültekin & Miller 2012; Kocsis et al. 2012; Tanaka & Haiman 2013; Roedig et al. 2014, however see Farris et al. 2015b for a simulation where notches become obscured). Thus, it is possible to use PSO J334’s SED to search for evidence of minidisks. Specifically, Roedig et al. (2014) derive analytical calculations of the specific luminosity integrated from the circum-binary disk and the two mini-disks, where the primary and secondary BHs are accreting material at rates $\dot{M}_1 = f_1 \dot{M}$ and $\dot{M}_2 = f_2 \dot{M}$. Here \dot{M}_1 and \dot{M}_2 are the mass accretion rates of the primary and secondary, and \dot{M} is the circum-binary accretion rate. Further, they assume the circum-binary disk is in inflow equilibrium (i.e., $f_1 + f_2 = 1$) and take into account a hardening factor $g = 1.7$. The emergent spectrum may be hardened by a factor g due to the majority of the disk laying in a regime in which electron scattering opacity dominates absorption opacity (Shimura & Takahara 1995). Lastly, they assume that there is a sharp surface density cut-off at the inner edge of the circum-binary disk and the outer edges of the mini-disks. For this particular model, they find that a spectral depression tends to occur in the SED between $\sim kT_{\text{notch}} - 15kT_{\text{notch}}$, where T_{notch} is the characteristic temperature of the accretion disk at a radius $r_{\text{notch}} \sim a$ and is approximately $2^{3/4} T_{\text{circum,edge}}$ (see their equation 3). T_{notch} is evaluated at a radius that lies between the hottest point in the circum-binary accretion disk (which is truncated to $\sim 2a$) and the coldest point in the minidisk (which extends to $\sim a/2$). We expect very little thermal radiation at the energy corresponding to the deepest point of the notch, which is centered at $E \simeq 4kT_{\text{notch}}$.

For PSO J334, we calculate $T_{\text{notch}} \approx 19000 \pm 7000$ K, translating to an observable notch in the SED between 500–7000 Å, where the deepest point is predicted to occur at $\lambda_{\text{notch}} \approx 1900^{+1200}_{-500}$ Å. In Fig. 2 we indicate the position of λ_{notch} with respect to PSO J334’s SED. We use the analytical calculations in Roedig et al. (2014) to analyze how the SED shape is affected by the presence of a notch, for various parameters of q , f_1 , and f_2 . The continuum for the notch is estimated by approximating the Shang et al. (2011) SED between 500 Å and 7000 Å with a straight line. Three examples of notched SEDs are shown in Fig. 2. Our SED is reasonably resolved throughout the expected frequency range of a spectral notch, and the data appear nominally closer to the standard Shang et al. (2011) SED model.

We note that it is possible the mass ratio of PSO J334 falls much below $q \simeq 0.3$ (Liu et al. 2015). Specifically, for the case of $q \leq 0.1$ it is likely that any notch in the SED will have a different shape from the analysis above. We may expect λ_{notch} to occur at shorter wavelengths and the deepest portion of the notch to be even lower; this is a result of the primary BH’s accretion flow barely contributing to the total SED (i.e., $f_2 \gg f_1$; Roedig et al. 2014). High S/N spectroscopy between 500 Å and 7000 Å, along with dense FUV observations, are required for a more robust analysis on possible notches in the SED.

4.2.3. Hard X-ray Emission from Minidisks

As a result of the expected supersonic motions of streams that are accreting onto the minidisks from the circum-binary disk, shocks are predicted as the streams hit the minidisk edges. It has been shown that these shocks should manifest in an excess of hard X-ray emission in the SED (Roedig et al. 2014; Farris et al. 2015b,a). Roedig et al. (2014) show that the post-shock temperature, T_{ps} , of accreting streams is usually in excess of 10^9 K, with $T_{\text{ps}} \propto (a/100R_G)^{-1} (1+q^{0.7})^{-1}$ (assuming the secondary is the main accretor). However, cooling is expected to rapidly set in such that the resultant emission is between 50 and 200 keV. These results agree with simulations presented in Farris et al. (2015a), where excess emission from stream shocking is ~ 10 times higher than a normal AGN SED between 10 and 100 keV. Given that Farris et al. (2015a) assume a mass ratio $q = 1.0$, PSO J334 may be expected to have an excess of emission at an even energy higher if the mass ratio of the binary-AGN is much lower than unity.

Our rest-frame ~ 0.9 to 24.5 keV *Chandra* spectrum shows no evidence of excess hard X-ray emission with respect to an absorbed power-law model. However, as argued above, it is likely that any excess X-ray emission would reside above our *Chandra* observation’s energy range. We consider possible temperatures for the stream-shocking emission from PSO J334, given an assumed semi-major axis $a = 56R_G$ and a range of mass ratios $0.01 < q < 1.0$. Adopting the assumption from Roedig et al. (2014) that a mass ratio $q \simeq 1.0$ and semi-major axis $a = 100R_G$ will result in an additional Wien-like spectrum with peak energy $\simeq 100$ keV, we predict that any excess emission from stream-shocking in PSO J334 could peak between rest-frame 180–340 keV, or observed-frame 60–110 keV. Because of the approximate nature of these calculations, we can only make an estimate for detectability with *NuSTAR*. However, if we assume a similar photon index in the 60–110 keV energy range as found in our 2–10 keV spectral fit, and assume that stream-shocking will result in an excess of emission ~ 10 times higher than a normal AGN SED in this energy range, the count rate in *NuSTAR* is expected to be close to $\sim 1 \times 10^{-5}$ counts per second. Thus, such emission will not be easily detected by *NuSTAR*. We note that a more detailed analysis on the post-shock temperature evolution, including relevant cooling mechanisms such as pair production, will be necessary in order to determine the resultant hard X-ray spectrum expected from stream shocking.

5. CONCLUSIONS

In this work, we present the first targeted X-ray observation of PSO J334, a candidate binary-AGN system, with the aim to uncover the true accretion nature of the quasar. If a binary-AGN system with a separation of $28R_S$ (Liu et al. 2016), PSO J334 is well into the gravitational-wave dominated regime and should be undergoing circum-binary accretion. Simulations show that two main types of circum-binary accretion disk morphologies can be expected: a cavity, where emission is truncated blueward of the wavelength associated with the temperature of the innermost ring due to a mostly empty accretion disk, or minidisks, where there is substantial accretion onto one or both of the members of the binary, each with their own shock-heated thin disk. Cavities and minidisks are expected to exhibit different behavior in the high-energy regime. Specifically, if the accretion disk of PSO J334 contains a cavity it is very likely that no, or very little, X-ray emission is expected. Further, if PSO J334 is accreting

via minidisks, we may expect to see a notch in the SED or an excess of hard X-ray emission above ≥ 100 keV. Our 40 ks *Chandra* observation allows for the opportunity to discern between a single- or binary-AGN system, and if a binary, can characterize the type of circum-binary accretion. The main results and implications of this work can be summarized as follows:

- (1) We find that PSO J334's X-ray emission is best explained by a mildly absorbed power-law with intrinsic $N_H = 0.91^{+4.84}_{-0.89} \times 10^{22} \text{ cm}^{-2}$ and $\Gamma = 2.02^{+0.83}_{-0.39}$, with an observed 2–10 keV flux of $3.20^{+0.9}_{-1.1} \times 10^{-14} \text{ erg cm}^{-2} \text{ s}^{-1}$, or rest-frame 2–10 keV luminosity of $9.40^{+1.4}_{-1.1} \times 10^{44} \text{ erg s}^{-1}$ at $z = 2.06$ (assuming isotropic emission). We fit a broken power-law model, which may originate from a binary system where both SMBHs are accreting with their own minidisk, and find at a 95% confidence level that the spectrum does not need an additional photon index to explain its shape.
- (2) We construct a radio–X-ray SED for PSO J334, using new VLBA data (Mooley et al. 2017); archival *WISE*, UKIDSS, Pan-STARRS1 (Liu et al. 2015), and *GALEX* data; and our new *Chandra* data. We find the SED agrees well with the composite non-blazar AGN SEDs presented in Shang et al. (2011).
- (3) Other analyses, such as comparing IR *WISE* colors to the empirical “AGN box” presented in Jarrett et al. (2011) and calculating the mass of the accreting system via the FP, further reflects the similarity of PSO J334 with respect to normal AGN.
- (4) We calculate the temperature at the inner edge of a possible circum-binary disk and find that no, or very little, emission is expected beyond $\sim 2500^{+1600}_{-700} \text{ \AA}$. However from our *Chandra* observation we can verify that the intensity at energies above 2500 Å is consistent with the expected upscattered UV emission from a normal AGN disk. We conclude that the X-ray emission of PSO J334 is incompatible with the cavity accretion mode.
- (5) We find no gap in the SED expected from the missing emission between $R_{\text{circum,edge}}$ and R_{tidal} , predicted to be between 500–7000 Å, for mini-disk accretion models. We note that it is possible that a notch exists within the data but is undetected given the resolution of our SED.
- (6) If PSO J334 is accreting via minidisks, then we may expect a detectable excess of hard X-ray emission above $E \geq 100$ keV, depending on the mass ratio of the system and the various time-dependent cooling processes of the post-shock photons. Our rest-frame ~ 0.9 to 24.5 keV *Chandra* spectrum shows no evidence of excess hard X-ray emission with respect to an absorbed power-law model, however we predict that any excess emission from stream-shocking should peak between rest-frame 180–340 keV, or observed-frame 60–110 keV. Near-future observations are unlikely to detect a possible excess of emission at these higher energies.

We have shown through various analyses that there is an absence of evidence supporting PSO J334 as a binary-AGN system. Specifically, we find no compelling evidence supporting PSO J334 as a binary-AGN system containing a cavity, or a binary-AGN system with mass ratios $q \geq 0.1$. However, because of the small number of currently promising binary-AGN candidates, it is most likely that the best method to distinguish a binary-AGN from a single-AGN has yet to be identified. Regarding the true nature of PSO J334, a stronger ar-

gument in either direction can be made with i) a high S/N spectrum between 500–7000 Å to allow for a more robust analysis on whether PSO J334 agrees better with the standard AGN-model or a notched-SED, and ii) a FUV spectrum that will allow for a better analysis of a possible binary-AGN system with mass ratios much below $q = 0.1$. As well, hard X-ray observations targeting excess emission expected from stream-shocking will be important for determining the accretion mode of the quasar.

We thank the referee for helpful and constructive comments. AF acknowledges support provided by the Rackham Graduate School Conference Grant and the National Space Grant Foundation's John Mather Nobel Scholarship Program. KG and MR acknowledge support provided by the National Aeronautics and Space Administration through Chandra Award Number GO6-17104X issued by the Chandra X-ray Observatory Center, which is operated by the Smithsonian Astrophysical Observatory for and on behalf of the National Aeronautics Space Administration under contract NAS8-03060. This research has made use of the NASA/IPAC Extragalactic Database (NED) which is operated by the Jet Propulsion Laboratory, California Institute of Technology, under contract with the National Aeronautics and Space Administration. This research has made use of NASA's Astrophysics Data System.

REFERENCES

- Arnaud, K. A. 1996, in *Astronomical Society of the Pacific Conference Series 101, Astronomical Data Analysis Software and Systems V*, ed. G. H. Jacoby & J. Barnes, 17
- Baker, J. G., Boggs, W. D., Centrella, J., Kelly, B. J., McWilliams, S. T., Miller, M. C., & van Meter, J. R. 2008, *ApJ*, 682, L29
- Bansal, K., Taylor, G. B., Peck, A. B., Zavala, R. T., & Romani, R. W. 2017, *ApJ*, 843, 14
- Becker, R. H., et al. 2001, *ApJS*, 135, 227
- Begelman, M. C., Blandford, R. D., & Rees, M. J. 1980, *Nature*, 287, 307
- Berczik, P., Merritt, D., Spurzem, R., & Bischof, H.-P. 2006, *ApJ*, 642, L21
- Berentzen, I., Preto, M., Berczik, P., Merritt, D., & Spurzem, R. 2009, *ApJ*, 695, 455
- Cash, W. 1979, *ApJ*, 228, 939
- Comerford, J. M., et al. 2009, *ApJ*, 698, 956
- Cuadra, J., Armitage, P. J., Alexander, R. D., & Begelman, M. C. 2009, *MNRAS*, 393, 1423
- Cutri, R. M., et al. 2013, *Explanatory Supplement to the AllWISE Data Release Products*, Tech. rep.
- D'Orazio, D. J., Haiman, Z., & MacFadyen, A. 2013, *MNRAS*, 436, 2997
- D'Orazio, D. J., Haiman, Z., & Schiminovich, D. 2015, *Nature*, 525, 351
- Dotti, M., Colpi, M., Haardt, F., & Mayer, L. 2007, *MNRAS*, 379, 956
- Drake, A. J., et al. 2009, *ApJ*, 696, 870
- Ellison, S. L., Secrest, N. J., Mendel, J. T., Satyapal, S., & Simard, L. 2017, preprint (1705.05465)
- Elvis, M., et al. 1994, *ApJS*, 95, 1
- Eracleous, M., Boroson, T. A., Halpern, J. P., & Liu, J. 2012, *ApJS*, 201, 23
- Escala, A., Larson, R. B., Coppi, P. S., & Mardones, D. 2005, *ApJ*, 630, 152
- Fabbiano, G., Wang, J., Elvis, M., & Risaliti, G. 2011, *Nature*, 477, 431
- Farris, B. D., Duffell, P., MacFadyen, A. I., & Haiman, Z. 2015a, *MNRAS*, 447, L80
- . 2015b, *MNRAS*, 446, L36
- Foord, A., Gallo, E., Hodges-Kluck, E., Miller, B. P., Baldassare, V. F., Gültekin, K., & Gnedin, O. Y. 2017, *ApJ*, 841, 51
- Gallo, E., Treu, T., Jacob, J., Woo, J.-H., Marshall, P. J., & Antonucci, R. 2008, *ApJ*, 680, 154
- Gallo, E., Treu, T., Marshall, P. J., Woo, J.-H., Leipski, C., & Antonucci, R. 2010, *ApJ*, 714, 25
- Gezari, S., et al. 2013, *ApJ*, 766, 60
- Gold, R., Paschalidis, V., Etienne, Z. B., Shapiro, S. L., & Pfeiffer, H. P. 2014, *Phys. Rev. D*, 89, 064060
- Graham, M. J., et al. 2015, *Nature*, 518, 74
- Greene, J. E., & Ho, L. C. 2005, *ApJ*, 630, 122
- Gültekin, K., Cackett, E. M., King, A. L., Miller, J. M., & Pinkney, J. 2014, *ApJ*, 788, L22
- Gültekin, K., Cackett, E. M., Miller, J. M., Di Matteo, T., Markoff, S., & Richstone, D. O. 2009, *ApJ*, 706, 404
- Gültekin, K., & Miller, J. M. 2012, *ApJ*, 761, 90

- Heinis, S., et al. 2016a, *ApJ*, 826, 62
 ———. 2016b, *ApJ*, 821, 86
 Hough, D. H. 2013, in *European Physical Journal Web of Conferences* 61, European Physical Journal Web of Conferences, 08009
 Ivezić, Ž., et al. 2002, *AJ*, 124, 2364
 Jarrett, T. H., et al. 2011, *ApJ*, 735, 112
 Jovanović, P., Borka Jovanović, V., Borka, D., & Popović, L. Č. 2016, *Ap&SS*, 361, 75
 Kaiser, N., et al. 2010, in *Proc. SPIE7733, Ground-based and Airborne Telescopes III*, 77330E
 Kalberla, P. M. W., Burton, W. B., Hartmann, D., Arnal, E. M., Bajaja, E., Morras, R., & Pöppel, W. G. L. 2005, *A&A*, 440, 775
 Kellermann, K. I., Sramek, R., Schmidt, M., Shaffer, D. B., & Green, R. 1989, *AJ*, 98, 1195
 Kewley, L. J., Groves, B., Kauffmann, G., & Heckman, T. 2006, *MNRAS*, 372, 961
 Khan, F. M., Holley-Bockelmann, K., Berczik, P., & Just, A. 2013, *ApJ*, 773, 100
 Kocsis, B., Haiman, Z., & Loeb, A. 2012, *MNRAS*, 427, 2680
 Koss, M. J., et al. 2015, *ApJ*, 807, 149
 Lawrence, A., et al. 2007, *MNRAS*, 379, 1599
 Lehto, H. J., & Valtonen, M. J. 1996, *ApJ*, 460, 207
 Leighly, K. M., Terndrup, D. M., Gallagher, S. C., & Lucy, A. B. 2016, *ApJ*, 829, 4
 Liu, T., et al. 2016, *ApJ*, 833, 6
 ———. 2015, *ApJ*, 803, L16
 Lodato, G., Nayakshin, S., King, A. R., & Pringle, J. E. 2009, *MNRAS*, 398, 1392
 Lousto, C. O., & Zlochower, Y. 2013, *Phys. Rev. D*, 87, 084027
 Mayer, L., Kazantzidis, S., Madau, P., Colpi, M., Quinn, T., & Wadsley, J. 2007, *Science*, 316, 1874
 Merritt, D., Milosavljević, M., Favata, M., Hughes, S. A., & Holz, D. E. 2004, *ApJ*, 607, L9
 Miller, B., Gallo, E., Treu, T., & Woo, J.-H. 2012a, *ApJ*, 747, 57
 ———. 2012b, *ApJ*, 745, L13
 Miller, B. P., Gallo, E., Greene, J. E., Kelly, B. C., Treu, T., Woo, J.-H., & Baldassare, V. 2015, *ApJ*, 799, 98
 Milosavljević, M., & Merritt, D. 2003a, *ApJ*, 596, 860
 ———. 2003b, in *American Institute of Physics Conference Series* 686, The Astrophysics of Gravitational Wave Sources, ed. J. M. Centrella, 201
 Milosavljević, M., & Phinney, E. S. 2005, *ApJ*, 622, L93
 Mooley, K. P., Wrobel, J. M., Anderson, M. M., & Hallinan, G. 2017, preprint (1703.10227)
 Mooley, K. P., et al. 2016, *ApJ*, 818, 105
 Paczynski, B. 1977, *ApJ*, 216, 822
 Panessa, F., Barcons, X., Bassani, L., Cappi, M., Carrera, F. J., Ho, L. C., & Pellegrini, S. 2007, *A&A*, 467, 519
 Peters, P. C. 1964, *Physical Review*, 136, 1224
 Plotkin, R. M., Gallo, E., Miller, B. P., Baldassare, V. F., Treu, T., & Woo, J.-H. 2014, *ApJ*, 780, 6
 Popović, L. Č. 2012, *NewAr*, 56, 74
 Rezzolla, L., Barausse, E., Dorband, E. N., Pollney, D., Reisswig, C., Seiler, J., & Husa, S. 2008, *Phys. Rev. D*, 78, 044002
 Richards, G. T., et al. 2006, *AJ*, 131, 2766
 Roedig, C., Krolik, J. H., & Miller, M. C. 2014, *ApJ*, 785, 115
 Roedig, C., Sesana, A., Dotti, M., Cuadra, J., Amaro-Seoane, P., & Haardt, F. 2012, *A&A*, 545, A127
 Runnoe, J. C., Brotherton, M. S., & Shang, Z. 2012, *MNRAS*, 422, 478
 Schlafly, E. F., & Finkbeiner, D. P. 2011, *ApJ*, 737, 103
 Shang, Z., et al. 2011, *ApJS*, 196, 2
 Shimura, T., & Takahara, F. 1995, *ApJ*, 445, 780
 Simić, S., & Popović, L. Č. 2016, *Ap&SS*, 361, 59
 Stern, D., et al. 2012, *ApJ*, 753, 30
 Stocke, J. T., Morris, S. L., Weymann, R. J., & Foltz, C. B. 1992, *ApJ*, 396, 487
 Tanaka, T., Menou, K., & Haiman, Z. 2012, *Monthly Notices of the Royal Astronomical Society*, 420, 705
 Tanaka, T. L. 2013, *MNRAS*, 434, 2275
 Tanaka, T. L., & Haiman, Z. 2013, *Classical and Quantum Gravity*, 30, 224012
 Telfer, R. C., Zheng, W., Kriss, G. A., & Davidsen, A. F. 2002, *ApJ*, 565, 773
 Valtonen, M. J., et al. 2008, *Nature*, 452, 851
 Vanden Berk, D. E., et al. 2001, *AJ*, 122, 549
 Vaughan, S., Uttley, P., Markowitz, A. G., Huppenkothen, D., Middleton, M. J., Alston, W. N., Scargle, J. D., & Farr, W. M. 2016, *MNRAS*, 461, 3145
 Volonteri, M., Haardt, F., & Madau, P. 2003, *ApJ*, 582, 559
 Volonteri, M., Lodato, G., & Natarajan, P. 2008, *MNRAS*, 383, 1079
 Wang, J. X., Malhotra, S., Rhoads, J. E., & Norman, C. A. 2004, *ApJ*, 612, L109
 White, S. D. M., & Rees, M. J. 1978, *MNRAS*, 183, 341
 Yu, Q. 2002, *MNRAS*, 331, 935
 Yuan, H. B., Liu, X. W., & Xiang, M. S. 2013, *MNRAS*, 430, 2188